Shear-induced diffusion and rheology of noncolloidal suspensions: Time scales and particle displacements

Victor Breedveld, Dirk van den Ende,[a] Robert Jongschaap, and Jorrit Mellema
Twente Institute of Mechanics, Rheology Group, Department of Applied Physics, University of Twente, P.O. Box 217, 7500 AE Enschede, The Netherlands

(Received 31 May 2000; accepted 23 January 2001)

The shear-induced self-diffusion and rheology of concentrated suspensions of noncolloidal hard spheres have been studied experimentally. The combined results provide an interesting physical picture. The projection of the trajectories of individual particles on the vorticity (z)–velocity (x) plane were determined through particle tracking. The particle trajectories turned out to be very useful for gaining qualitative insight into the microscopic particle motion. However, the technique is less suitable to obtain quantitative information. For a quantitative analysis of the particle displacements we measured the evolution of the ensemble averaged displacements as a function of time. The statistical analysis revealed two diffusion regimes, where $\langle \Delta z \Delta z \rangle \sim \dot{\gamma} \Delta t$. For large strain values ($\dot{\gamma}\Delta t > 1$) long-time self-diffusion was observed. The associated diffusion coefficient $\hat{D}_\infty$ is in excellent agreement with literature data on shear-induced self-diffusion. On very short times ($\dot{\gamma}\Delta t \ll 1$) a novel diffusive regime was discovered, characterized by a diffusion coefficient $\hat{D}_0$, which is significantly smaller than $\hat{D}_\infty$ and grows monotonically with ϕ. $\hat{D}_0$ is detected on time scales on which the particle configuration is not changed significantly and thus it must represent the fluctuating motion of particles in the ''cage'' formed by their nearest neighbors. Finally, the rheology was studied with steady shear and oscillatory rheometry. The dynamic measurements in a controlled stress rheometer revealed that the viscoelastic response of the suspension is determined mainly by the amplitude of deformation. At small strain amplitudes $\gamma_0 < 1$, the response is linear and a dynamic viscosity η' is found, which is in excellent agreement with the high frequency limit η'_∞ as reported in literature for colloidal hard sphere suspensions. Around $\gamma_0 = 1$ the ''cage'' around a particle is deformed and a shear-induced microstructure is built. This leads to $O(a)$ displacements of the particles and the viscoelastic response becomes strongly nonharmonic. Although the effect persists at large amplitudes, it becomes relatively small for $\gamma_0 \gg 1$. The microstructure is rearranged immediately after flow reversal and remains unchanged for the larger part of the period of oscillation. As a result a pseudolinear viscoelastic regime is found with a viscosity close to steady shear viscosity. Experiments show a correlation between the time scales controlling the $\hat{D}_0/\hat{D}_\infty$ diffusive behavior and the ones controlling the shear-induced changes in particle configuration as probed by the rheological measurements. © *2001 American Institute of Physics.*
[DOI: 10.1063/1.1355315]

I. INTRODUCTION

Shear-induced diffusion is an important phenomenon in the field of suspension rheology. It is one of the basic transport processes in concentrated suspensions and has significant influence on the macroscopic flow behavior of noncolloidal suspensions.[1] The underlying mechanism of shear-induced diffusion is formed by the velocity fluctuations of individual particles due to the changing configuration of all other particles. The macroscopic flow drives particles on adjacent streamlines toward each other and because of excluded volume effects the particles are forced to leave their streamlines. In concentrated suspensions the excluded volume effects result in net particle displacements. Although in principle hydrodynamic interactions are of deterministic nature, the changing configuration causes diffusive behavior in concentrated suspensions.

The driving force of shear-induced diffusion differs from the more familiar concept of Brownian diffusion, which is driven by thermal forces and plays an important role for smaller, colloidal, particles. Moreover, shear-induced diffusion occurs at very low Reynolds numbers, so that inertia is insignificant as opposed to the case of particle dispersion in turbulent flows.

Since the experimental work of Leighton and Acrivos[2,3] shear-induced diffusion has been studied experimentally, numerically, and theoretically by various research groups, both on the level of self-diffusion and collective or gradient diffusion (for a review see Davis[4]). In this paper we restrict ourselves to self-diffusion, which describes the velocity fluctuations of individual particles.

[a]Electronic mail: h.t.m.vandenende@tn.utwente.nl

Experimentally, shear-induced self-diffusion has been studied with a number of different techniques. Eckstein *et al.*[5] have introduced the method of observing long-time displacements of a single tracer particle in a Couette flow by recording its position after each full rotation. The technique was improved by Leighton and co-workers.[2,6] They also introduced measurements of diffusion in the vorticity (z) direction.

Recently, we have developed another technique, which monitors the motion of an ensemble of tracer particles over much shorter times and extracts shear-induced diffusion coefficients by means of spatial correlation procedures.[7,8] These measurements were also performed in a steady shear situation and reveal that for strain values roughly $\dot{\gamma}\Delta t > 1$ ($\dot{\gamma}\Delta t$ being the relevant dimensionless time) the particle motion becomes diffusive. The latest experimental studies in shear flow[6–8] are in good agreement and have provided a consistent picture of the experimental values of the long-time diffusion coefficients.

Now that reliable experimental data are available on long-time shear-induced diffusion coefficients, it seems feasible to investigate particle motion in sheared noncolloidal suspensions in more detail. Our technique offers the possibility to study the evolution of ensemble averaged particle displacements over a wide range of strain ($0.03 < \dot{\gamma}\Delta t < 3.5$). Thus we can focus on the regime where the transition to diffusive motion occurs ($\dot{\gamma}\Delta t \approx 1$). In addition the nature of particle motion for even smaller strain values can be studied. Since shear-induced self-diffusion in noncolloidal hard-sphere suspensions is induced by the changing configuration of the particles (the spatial distribution determines the velocity of individual particles under shear), the motion of individual particles probes the underlying microstructure.

Experimentally we have investigated particle motion and its relevant time scales in two different ways. Characteristic particle trajectories are presented in Sec. III. The trajectories have been determined by means of particle tracking and enable direct observation of the motion of individual particles. These particle paths are useful in developing a qualitative picture of the particle motion.

The trajectories, however, are not very suitable to collect quantitative information about the particle displacements, since the method is laborious and a large number of trajectories is required for accurate statistical analysis. Detailed information about the ensemble averaged displacements was therefore obtained with our correlation method, which was originally developed to measure long-time self-diffusion coefficients.[7] In Sec. IV the ensemble averaged data are evaluated to obtain the characteristic time scales of the particle motion.

Not only self-diffusion, but also rheology is governed by particle positions, often represented by the particle distribution function. In a noncolloidal suspension of hard spheres without interparticle forces in Stokes flow, the net hydrodynamic force on any particle must be zero (see, e.g., Brady and Bossis[9]). In that case the stresses and viscosities are determined directly by microstructure. In Sec. V we report on steady shear and dynamic rheometry. Similar experiments have been reported by Gadala-Maria and Acrivos[10] and Gondret *et al.*;[11] we have further explored the phenomena which they observed for our system. By combining the self-diffusion and rheological measurements for our suspensions a coherent picture arises. In Sec. VI we combine the results in an attempt to provide a consistent physical interpretation of our observations.

II. MATERIALS AND METHODS

For all experiments reported in this paper we made use of the experimental system described in a previous paper,[7] a refractive index and density matched suspension of PMMA particles suspended in a fluid mixture of demineralized water, zinc-II-chloride, and Triton X-100. The suspending fluid was measured to be Newtonian over the entire range of shear rates that could be covered by the rheometer (up to 100 s^{-1}) at a viscosity of 3.4 Pa s (23 °C). The particles (produced by ICI, class 4F, $\rho = 1.172$ g/ml) were sieved repeatedly to obtain a well-defined size fraction of diameter $90 \pm 15\ \mu$m. The sieved particles were density segregated to remove the particles with air bubbles. A small fraction of the particles was then colored with fabric dye (Rit, CPC International) and used as tracer particles to visualize particle motion.

Correlation experiments were performed to measure the ensemble averaged particle displacements and subsequently extract the long-time self-diffusion coefficients. The technique is based on spatial correlation of tracer particle positions in sequences of video images; for a detailed description of our experiments in a counter-rotating cone-plate apparatus we refer to our previous paper.[8] Here we reanalyze the results of the original study with the aim to collect detailed information about the microscopic nature of the diffusion process.

The video images used for the diffusion experiments could also be used to apply particle tracking. Thus the trajectories of individual tracer particles were determined over relatively long times. Our image grabbing system, consisting of charge-coupled device (CCD) camera, frame grabber, and PC, was able to capture sequences of maximally 200 images. The upper limit was set by the amount of RAM (256 Mbytes) in the frame grabbing PC. The actual physical length of the sequences—expressed in dimensionless strain units—depended on the interval time between consecutive images and on the shear rate, which were both varied. In this study we have collected time series in which particles could be tracked for as long as 50 strain units ($\dot{\gamma}\Delta t$). Sequences with shorter interval times were also analyzed to obtain a higher strain resolution.

The tracking procedure consisted of the following steps. First, suitable sequences were identified, in which a specific tracer particle remained within the camera window (1.10 by 0.83 mm with a viewing depth of 0.40 mm) during the entire sequence. The images of these series were then analyzed with a commercial software package for image analysis (OPTIMAS): the position of the tracer particle was determined manually by fitting a circular overlay to the particle contour. The position of the overlay was registered as a measure for the tracer position.

In spite of the software's sophisticated particle recognition algorithms the tracking procedure could not be auto-

mated. Not every image was of sufficiently high quality because of particle overlap and other image distortions. When measuring the self-diffusion[8] this effect was unimportant, since the ensemble statistics were not affected significantly by the odd missing tracer position. Particle tracking, however, requires accurate knowledge of the particle position at every moment in time. Omissions in the time series would seriously disrupt the trajectory. By performing the analysis manually even the positions of overlapping tracers could be determined accurately. As long as a significant part of the particle contour is visible, precise placement of the circular overlay is relatively easy. Furthermore, automatical particle tracking would require a clever algorithm to identify individual particles in subsequent images, which by eye is a simple task.

In order to determine the experimental errors of the manual particle tracking procedure, for a number of images the manual outcome was compared to the results of the automated image analysis algorithm which was employed in the diffusion experiments. The influence of the operator was also checked by having a small sample of images analyzed by different people. All in all the error in tracer position as measured with the manual procedure turned out to be no larger than 1 pixel, which was also the spatial resolution of the placement of the circular overlay.

The rheological properties of the suspensions were characterized using a controlled stress rheometer (Haake RheoStress RS150) equipped with a Couette geometry (inner and outer gap radius respectively 20.71 and 21.71 mm). Since the average particle diameter is 90 μm, the gap is on the small side according to the rheological rule of thumb that a minimum gap size of $\sim$15 particle diameters is required for reliable viscosity measurements. As a result, we cannot exclude wall slip in our system. Wall slip would have influenced our rheological experiments, leading to underestimated viscosity values.[12] However, a Couette geometry with larger gap was unavailable and we believe that our most important observations, the oscillatory measurements to be presented in Sec. V (Fig. 10), have not been affected by the limited gap size. This belief is supported by the fact that quantitatively identical results have been observed by other researchers in a wider Couette geometry with roughened walls where wall slip is unlikely to play a role.[13]

After loading the suspensions we applied preshear to eliminate the loading effects that have been reported under similar experimental conditions and that have been related to shear-induced gradient migration across the annular gap.[3] Stress sweeps were then applied to measure the flow curves and finally frequency sweeps were performed at constant stress values. The details on the chosen values of stress and frequency are given in Sec. V.

III. PARTICLE TRAJECTORIES

Direct visual observation is a natural approach when studying particle motion, especially for noncolloidal suspensions of 90 μm particles that can easily be visualized with standard optics. As described in Sec. II, video images were taken from concentrated refractive index matched suspensions with a small fraction of opaque tracer particles. Besides the diffusion measurements to be described in Sec. IV, the images could also be used to reconstruct trajectories of individual tracer particles.

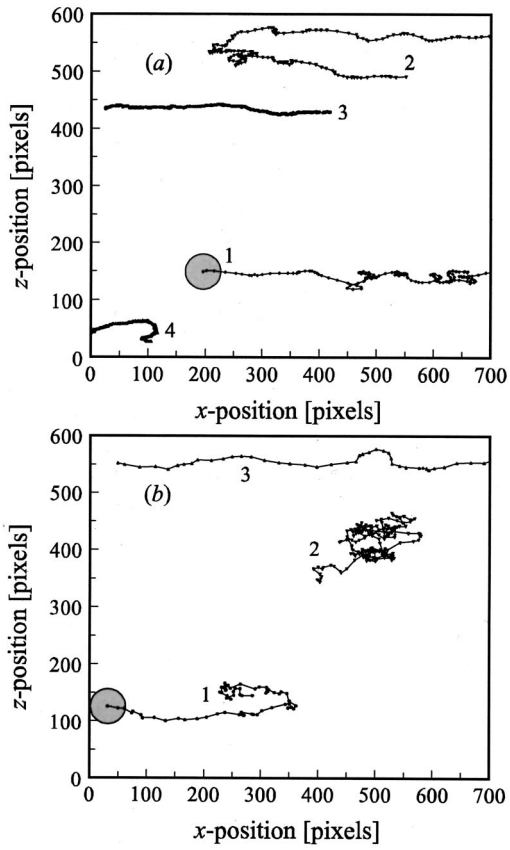

FIG. 1. Typical particle trajectories in the image window ($\Delta x-\Delta z$ plane) for volume fractions (a) $\phi=0.30$ and (b) $\phi=0.50$; strain $\dot{\gamma}\Delta t$ between consecutive points is 0.24 for all particles, except for particles 3 and 4 in (a), where the strain interval is 0.024. The paths have been shifted over arbitrary distances to minimize overlap and improve clarity.

To this purpose image sequences had to be identified for which tracers remained within the observation window for a much longer period than needed for the diffusion measurements. Sequences could be found with particle residence times as long as 50 strain units. Figure 1 shows typical particle trajectories in the $x-z$ plane for suspensions of 30% and 50% particle volume fraction. The strain step $\dot{\gamma}\Delta t$ between consecutive points in the graphs is 0.24 [for particles 3 and 4 in (a) the interval is 0.024]. Figure 1 represents the location of the particles on the CCD image (752×568 pixels). The measured positions were slightly shifted to minimize overlap of the trajectories and improve clarity. The average particle size (diameter 62 pixels) is indicated on the left-hand side.

The trajectories are replotted in Fig. 2, representing the particle coordinates as a function of time. The starting point of all trajectories was set to $\dot{\gamma}\Delta t=0$ and although some of the particles in Fig. 1 were followed for as long as 50 strain units, Fig. 2 has a maximum strain $\dot{\gamma}\Delta t=30$ so that the details can be distinguished. Note that different particles could be tracked over different lengths of time. The refined trajectories of the high resolution measurements of particles 3 and 4 in the 30% suspension ($\dot{\gamma}\Delta t=0.024$) did not alter the pic-

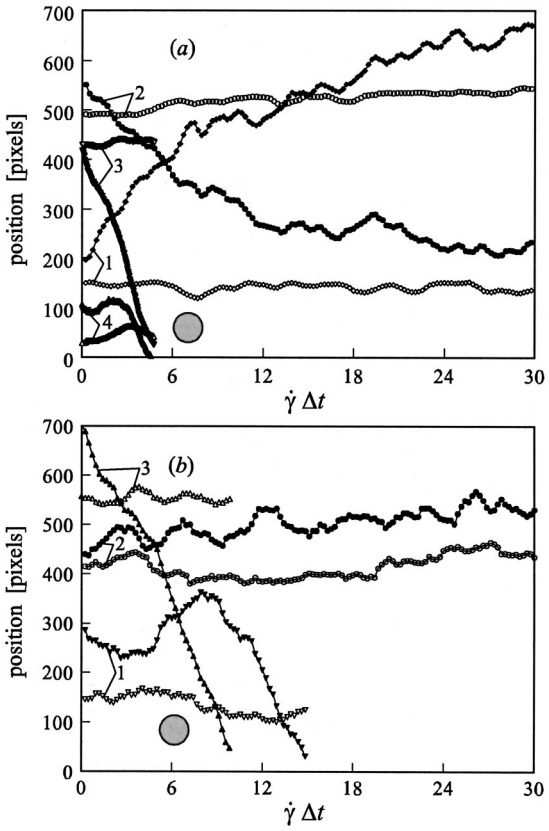

FIG. 2. Positions of individual particles as a function of dimensionless time $\dot{\gamma}\Delta t$ for (a) $\phi=0.30$, (b) $\phi=0.50$ in the x direction (closed symbols) and z direction (open symbols). Numbers correspond to Fig. 1 and the average particle size is indicated.

ture. All important observations can be made from the long (low resolution) trajectories with $\dot{\gamma}\Delta t=0.24$.

For both concentrations, the fluctuations in the x direction (closed symbols) are more pronounced than in the z direction (open symbols). The explanation is straightforward: displacements in the y direction (the unregistered out-of-plane velocity gradient direction) onto a different streamline inherently affect the convective motion in the velocity direction (x). Since the motion in the y direction is also of diffusive nature, the observed fluctuations along the x axis are the result of two processes: the fluctuations in x velocity itself and an additional coupling term due to fluctuations in the y direction.

The convective velocity field also causes the particles to occasionally drift over large distances along the x axis, i.e., when they are displaced onto a different streamline. Because of this, the particles can drift away from the zero velocity plane and (temporarily) disappear from the viewing window (e.g., particle 3 at both concentrations). On average, however, the particles should fluctuate around their original position, which is validated by the z data of Figs. 2(a) and 2(b).

The largest displacements in Fig. 2 are of $O(a)$ for both volume fractions and in both flow directions (a being the particle radius), thus confirming scaling ideas[2,14] which are based on the assumption that interactions will lead to displacements of the size of the particle. The present study provides experimental evidence in support of these predictions.

In particular the $O(a)$ displacements in the z direction are notable. Calculations of particle interactions in the dilute regime[15–17] have shown that displacements in the vorticity direction are considerably smaller than in the velocity gradient direction, irrespective of the mechanism responsible for braking the symmetry of two particle interactions in Stokes flow: particle roughness,[15] the presence of a third particle,[16] or a repulsive force.[17] As a consequence, the calculations in the dilute regime render highly anisotropic self-diffusion coefficients, $\hat{D}_{yy}/\hat{D}_{zz}\sim O(10)$, while experiments[6,8] and Stokesian dynamics calculations[18] in the concentrated regime both find $\hat{D}_{yy}/\hat{D}_{zz}\approx 2$. Taking into account that both theoretical (dilute) and Stokesian dynamics (concentrated) calculations show $O(a)$ displacements in the y direction, our experimental particle trajectories with $O(a)$ steps in the z direction (Fig. 2) are in good agreement with the data for concentrated suspensions. Apparently, additional effects must be incorporated in the theories for dilute suspensions to account for the relatively low experimental anisotropy.

Figures 1 and 2 reveal slight differences in particle motion at the two volume fractions. For $\phi=0.30$ the curves are very smooth, which is particularly clear in the z direction. The particle trajectories consist of a chain of successive displacements, which occur relatively slowly. In the highly concentrated 50% suspension the particles move more violently: the major displacements occur faster and are larger in amplitude. In between the large steps the particles keep wiggling around their location with a characteristic time that is shorter than the sampling interval. Occasionally, sudden stationary sections can be observed (e.g., x position of particle 2 around $\dot{\gamma}\Delta t=12$) as if the particle is trapped.

Although the trajectories provide useful insight into the motion of individual tracers, they are less suitable for a detailed quantitative analysis. The manual procedure is labor intensive and a significant number of paths would be needed for reliable statistics.

IV. SELF-DIFFUSION MEASUREMENTS

For a quantitative analysis of the particle motion we have switched to another observational level: the statistics of motion of a large ensemble of particles.

In recent years we have developed a correlation technique[7] for measuring self-diffusion coefficients in noncolloidal suspensions under shear. Without going into details, the experimental procedure essentially results in $\langle \Delta x \Delta x\rangle/a^2-\dot{\gamma}\Delta t$ graphs which show the ensemble averaged square displacement versus time. Both the displacement and time are made dimensionless by scaling with, respectively, the particle radius a and shear rate $\dot{\gamma}$. Linear scaling in these graphs indicates diffusive behavior and in that case the self-diffusion coefficients can be extracted directly from the slope of the linear regime, making use of the standard diffusion relation $\langle \Delta x \Delta x\rangle \sim 2D\Delta t$.

The transition to the linear (diffusive) regime is expected to depend on the underlying microstructure of the suspension. Therefore we believe that a detailed time scale analysis of the shear-induced diffusion data will yield valuable information about the microstructure in sheared suspensions. Fig-

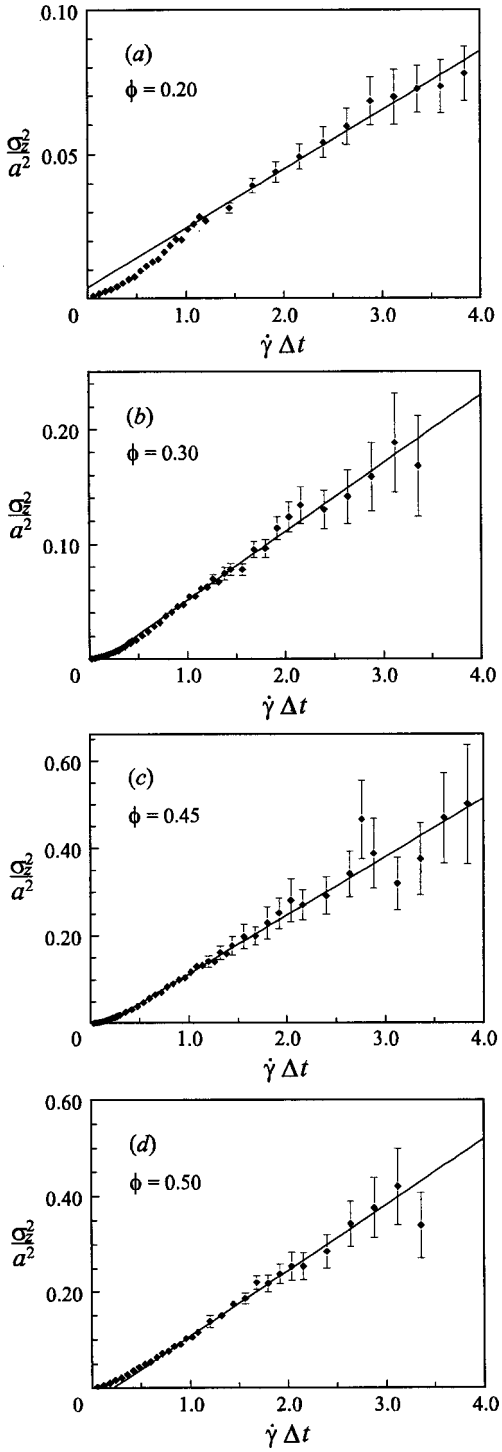

FIG. 3. Scaling of the average squared particle displacement σ_z^2/a^2 with dimensionless time $\dot{\gamma}\Delta t$ for (a) $\phi=0.20$, (b) $\phi=0.30$, (c) $\phi=0.45$, and (d) $\phi=0.50$; the lines represent the linear fit to the data points at long times.

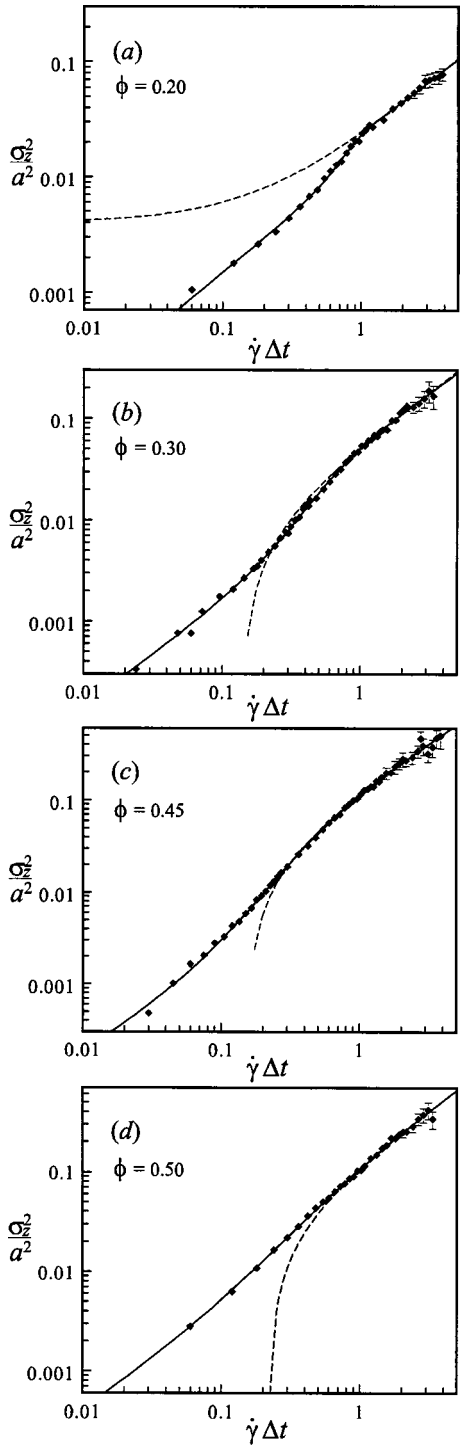

FIG. 4. Logarithmic version of Fig. 3; σ_z^2/a^2 vs $\dot{\gamma}\Delta t$ for (a) $\phi=0.20$, (b) $\phi=0.30$, (c) $\phi=0.45$, and (d) $\phi=0.50$; the dashed lines represent the linear fit to the data points at long times, the solid lines are the results of the empirical fit with Eq. (1).

ure 3 shows the results of the original correlation study[8] together with the long-time linear fits which were used to determine the long-time diffusion coefficient $\hat{D}$ (also dimensionless). The graphs all concern particle displacements in the vorticity (z) direction, which were also visible in the particle trajectories of Sec. III.

Figure 3 shows a transition to linear (diffusive) behavior that is most pronounced for the lowest volume fractions. The evolution from Figs. 3(a) to 3(d) suggests that the transition time decreases with increasing volume fraction ϕ.

In an attempt to find a quantitative criterion for the transition point the data were plotted on log–log scale, so that deviations of the linear fit could be observed more clearly. In Fig. 4 the logarithmic versions of Fig. 3 are presented together with the long-time linear fit and the results of an empirical model fit to be described in Sec. IV A. The deviations

of the data at short times from the long-time linear fit more pronounced, but it proved to be difficult to formulate an objective quantitative criterion to unambiguously determine the transition location.

The preferable approach for the characterization of the curves in Fig. 4 would have been the use of a theoretical model which contains the transition time as a fitting parameter. In this idealized situation standard statistical fitting routines could provide an unambiguous best fit value for the transition time. However, no theoretical model with a sound physical basis has been developed so far for shear-induced self-diffusion. Therefore we have chosen another solution.

A. Empirical model

We have attempted to find an empirical model that is capable of describing the curves of Fig. 4. Such a model should fulfill a number of important requirements in order to be scientifically acceptable. First of all, it should provide an accurate fit to the experimental data over the entire range of data. Second, it should involve a minimum number of free parameters and finally these parameters should have physical significance.

A closer look at the log–log plots of Fig. 4 discloses interesting scaling in the short-time regime. Within the classical framework of diffusion a transition might be expected from quadratic (''ballistic'') to linear (diffusive) scaling. However, the graphs do not display slope $+2$ at short times. Instead, the suggestion arises that the short-time scaling is also more or less linear, with slope $+1$. This observation implies the existence of two diffusive regimes: the long-time shear-induced self-diffusion which is characterized by the linear fit in Fig. 3 and an additional short-time diffusivity for $\dot{\gamma}\Delta t$ smaller than roughly 0.20. On intermediate time scales there is a smooth transition between the two diffusive regimes.

The above-mentioned considerations lead to the following empirical model to capture the observed phenomena:

$$\frac{\sigma^2}{a^2}=\frac{c_2\cdot\dot{\gamma}\Delta t}{1+\left(\frac{\dot{\gamma}\Delta t}{c_0}\right)^{c_1}}+\frac{(c_3\cdot\dot{\gamma}\Delta t+c_4)\left(\frac{\dot{\gamma}\Delta t}{c_0}\right)^{c_1}}{1+\left(\frac{\dot{\gamma}\Delta t}{c_0}\right)^{c_1}}, \tag{1}$$

where σ/a and $\dot{\gamma}\Delta t$ are the dimensionless peak width and time. In the limits of short and long times Eq. (1) converges to the asymptotes:

$$\frac{\sigma^2}{a^2}=c_2\cdot\dot{\gamma}\Delta t \quad \text{for} \quad \dot{\gamma}\Delta t\ll c_0, \tag{2}$$

$$\frac{\sigma^2}{a^2}=c_3\cdot\dot{\gamma}\Delta t+c_4 \quad \text{for} \quad \dot{\gamma}\Delta t\gg c_0. \tag{3}$$

The fit parameters can be interpreted as follows: the location of the transition (c_0), the strength of the transition (c_1), the short-time diffusion coefficient ($c_2=2\hat{D}_0$), the long-time diffusion coefficient ($c_3=2\hat{D}_\infty$), and the off-set of the linear long-time fit (c_4). Equation (1) is similar to the well-known Cross model, often used to characterize shear-thinning fluids with two viscosity plateaus.[19]

Equation (1) was used to parametrize the data by means of a standard least squares nonlinear fitting routine. Since the linear fits in Fig. 3 show that the offset of the long-time linear fit only differs significantly from 0 at high volume fractions ($\phi>0.35$), parameter c_4 was used in Eq. (1) only if it had a significant and meaningful contribution to the convergence of the fitting routine. The fit procedure was carried out with $1/\epsilon^2$ as weight factor, ϵ being the statistical standard deviation of σ^2/a^2 that was also used for the error bars in Figs. 3 and 4. In turn these errors have been obtained from nonlinear Gaussian fits.[8]

B. Fit parameters

The results of the empirical model fit are presented in Fig. 4 as the solid curves. It can be concluded that the proposed model describes the data surprisingly well over the full range of time and volume fraction.

Although the proposed model is of empirical nature, its parameters have a clear physical meaning and their dependence on particle volume fraction ϕ, as presented in Fig. 5, can serve as a starting point to gain physical insight into the nature of the processes that take place in concentrated suspensions under shear. The error bars in the graphs are purely the result of an external statistical estimation, obtained from the covariance matrix of the nonlinear fit. It provides an explanation for the fact that some of the data points (e.g., c_0 for $\phi=0.45$) have unrealistically small errors in comparison to the rest of the data points. Nevertheless, this error estimate is the only available objective measure of the parameter reliability and regarding the empirical nature of our model it seemed appropriate to present those values.

Of the fitting parameters, c_2 and c_3 are directly related to the physical quantities $\hat{D}_0$ and $\hat{D}_\infty$, respectively, a short- and long-time diffusion coefficient [Eq. (2)]. The dependence of c_3 on ϕ should be identical to that of the long-time self-diffusion coefficient $\hat{D}_{zz}$, which was determined by using the long-time linear fit of Fig. 3.[8] This requirement is indeed satisfied.

The existence of a short-time diffusion regime, however, has not been reported before. As far as we are aware no previous experimental technique has been capable of measurements on such short time scales and no detailed analysis of numerical simulations in this regime has been reported so far, although it should be relatively straightforward to retrieve the necessary data from standard simulation runs.

Although for the highest volume fractions the short-time linear regime lies outside the accessible time window, the quality of the fit with Eq. (1) and the data for $\phi=0.20$ and 0.30 provide strong evidence that short-time diffusivity indeed exists at all volume fractions. The corresponding diffusion coefficient, $\hat{D}_0=0.5\cdot c_2$, exhibits a ϕ dependence that strongly differs from the behavior of $\hat{D}_\infty$. Although the standard deviations are significant because of the limited amount of data at short times, especially for $\phi=0.50$, $\hat{D}_0$ seems to grow continuously with increasing ϕ, whereas $\hat{D}_\infty$ increases strongly for intermediate volume fractions, followed by a plateau above $\phi=0.35$ and an apparent decrease at even

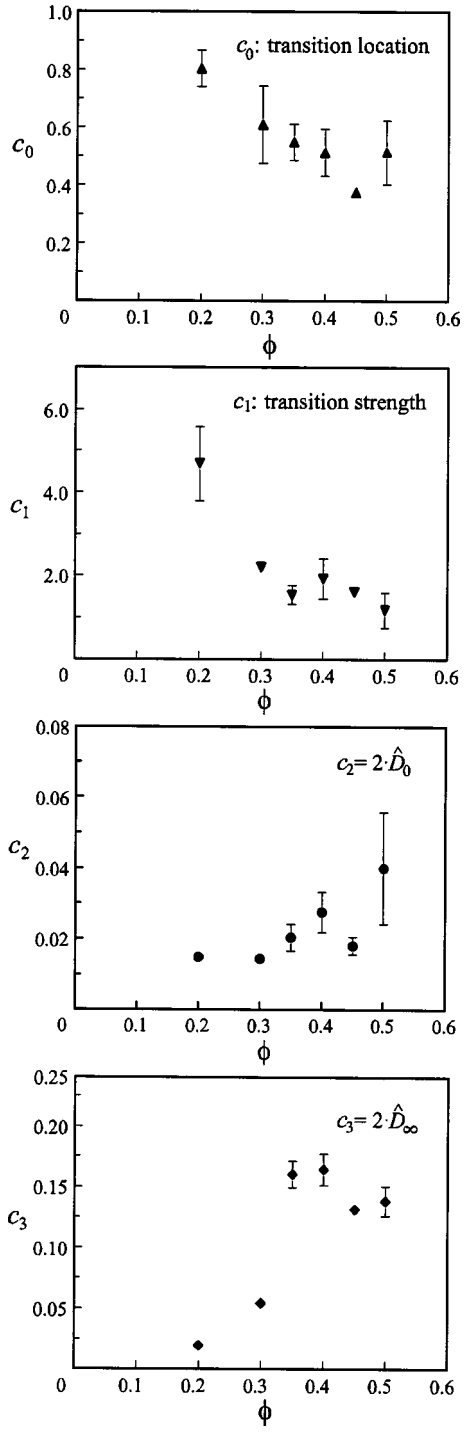

FIG. 5. Fit parameters of Eq. (1) as a function of ϕ.

higher volume fractions (reported as well by Phan and Leighton[6]).

The parameters c_0 and c_1 are somewhat more difficult to interpret. They characterize the transition between the two diffusion regimes through its slope (c_1) and location (c_0). For the development of a physical picture of the microscopic processes, it seems more useful to define two transition times, $\hat{\tau}_0$ and $\hat{\tau}_\infty$, which, respectively, mark the end of short-time and the onset of long-time diffusion, expressed in dimensionless strain units.

The definitions of $\hat{\tau}_0$ and $\hat{\tau}_\infty$ that we have chosen are

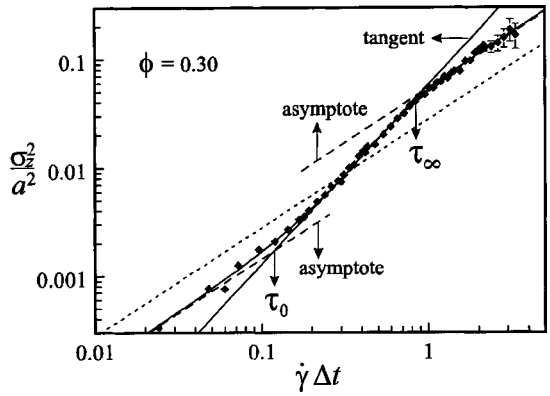

FIG. 6. Definition of the characteristic dimensionless times $\hat{\tau}_0$ and $\hat{\tau}_\infty$; the dashed lines denote the asymptotes, the dotted line the intermediate line, and the thin curve the fit function Eq. (1); the thick line represents the log–log tangent at the intercept.

illustrated in Fig. 6. The characteristic times are determined as follows: First, in the log–log plot (Fig. 4) the linear asymptotes of Eq. (2) are drawn and used to construct an additional line in between. The intersect of this intermediate line with the model fit [Eq. (1)] is then determined analytically and at the intersection point the tangent of the fit function (straight line in the log–log plot) is calculated. Finally, the intersects of the tangent with the asymptotes can be computed and these points are called $\hat{\tau}_0$ and $\hat{\tau}_\infty$.

The values of $\hat{\tau}_0$ and $\hat{\tau}_\infty$ were calculated for all volume fractions and are plotted in Fig. 7. The logarithmic scale was chosen to enable direct comparison of the two times, which differ by an order of magnitude. The error bars in Fig. 7 are the result of a rigorous analysis of the propagation of errors: For the fit parameters c_0 to c_4 the influence of $\langle \delta c_n^2 \rangle$ and $\langle \delta c_n \delta c_m \rangle$ on the values for $\hat{\tau}_0$ and $\hat{\tau}_\infty$ was calculated.

Within the experimental errors, which are significant especially for $\phi = 0.50$, the longest time scale, $\hat{\tau}_\infty$, is constant at $\dot{\gamma}\Delta t \sim 1$ over the full range of volume fractions, indicated by the dashed line.

The shortest time scale, $\hat{\tau}_0$, is an order of magnitude smaller and decreases with ϕ. Simple hand-waving arguments can be used to estimate an upper limit for $\hat{\tau}_0$. The point where short-time diffusion ends and long-time diffusion starts to dominate particle motion, here characterized by

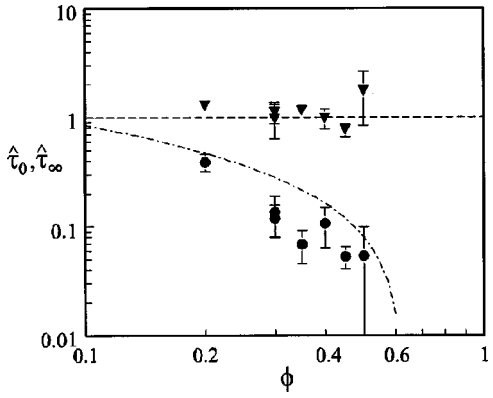

FIG. 7. Transition times (●) $\hat{\tau}_0$ and (▼) $\hat{\tau}_\infty$ as a function of ϕ; (— — —) represents $\hat{\tau} = 1$ and (-·-) Eq. (4) with $\phi_{max} = 0.63$.

$\hat{\tau}_0$, should be smaller than the affine shear deformation where particles directly interact with their nearest neighbors. This deformation can be approximated by δ/a with a the particle radius and δ the space around a particle in the ''cage'' formed by its neighbors. Assuming a homogeneous distribution of monodisperse particles, δ/a can be estimated by means of

$$\frac{\delta}{a}=\left(\frac{\phi_{\max}}{\phi}\right)^{1/3}-1, \tag{4}$$

where $\phi_{\max}$ denotes the maximum particle volume fraction. In Fig. 7 the curve (dash-dotted) has been drawn for $\phi_{\max}=0.63$ and provides a good upper limit to the data.

V. RHEOLOGICAL MEASUREMENTS

In addition to the direct observation of particles and a statistical analysis of the displacements we have investigated the rheological properties of the suspensions. Like shear-induced diffusion the rheological properties are the result of the underlying microscopic structure. Rheometry thus can be used as an independent method to experimentally address fundamental questions about the nature of the particle distribution in suspensions.

Our rheological experiments on concentrated noncolloidal suspensions were inspired by the work of Gadala-Maria and Acrivos[10,20] and Gondret *et al.*,[11] who observed peculiar behavior of the dynamic viscosity η' of noncolloidal suspensions. In order to relate the diffusion and rheology in our system, we have carried out similar experiments for our suspensions. Since the physical chemistry of suspensions is known to be of great influence on the rheology, it is nontrivial that our specific suspension should behave exactly like the materials used in previous studies.

Amongst other observations Gadala-Maria and Acrivos[10] discovered that the stress response in their controlled strain oscillations in both plate–plate and Couette configuration was linear at low strain amplitudes, but became highly nonlinear at amplitudes of $\gamma_0 \sim 1$ (see their Fig. 8).

Gondret *et al.*[11] reported that the dynamic viscosity of concentrated suspensions strongly depended on frequency and amplitude of the oscillations. As far as we can reconstruct from their paper, the experiments were carried out in a plate–plate geometry as well, which has the disadvantage that the strain distribution over the sample volume is highly nonuniform, being zero in the center and maximum at the edge of the plates.

Our rheological measurements were carried out in a controlled stress rheometer with Couette geometry (see Sec. II). Before performing dynamic measurements, first the flow curves of the suspensions were determined. Contrary to Gadala-Maria[10] we did not wait for the equilibrium value to be reached, as it has been shown that the gradual decrease of viscosity in their experiments can be attributed to shear-induced particle migration out of the Couette gap toward the stagnant fluid reservoir below the inner cylinder.[2] To prevent migration, which would decrease the particle volume fraction in the annular gap, we have presheared the suspensions only for a relatively short time as described in Sec. II in order to reach a reproducible starting point.

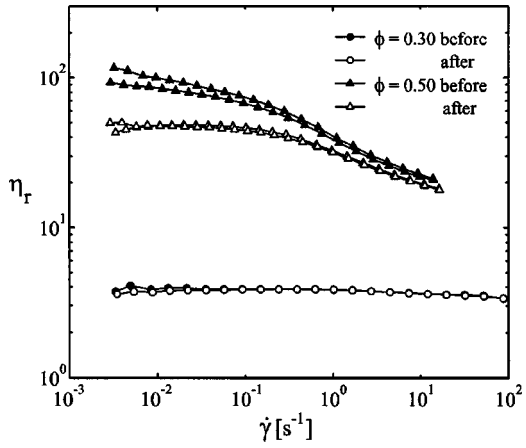

FIG. 8. Relative steady shear viscosity of concentrated noncolloidal suspensions as measured in a controlled stress Couette rheometer; (○) $\phi=0.30$ and (△) $\phi=0.50$; closed symbols were measured before and open symbols after the dynamic measurements, about 14 h later.

Due to particle migration out of the gap it was inevitable that in the course of our experiments the viscosity slightly decreased. We have been careful to minimize the applied shear in order to limit this effect. Fig. 8 presents the typical flow curves we found. As an estimate of the effect of migration flow curves are shown which were taken before and after our oscillatory experiments, the curves being separated by ~14 h of oscillations. The curves for 30% overlap nearly perfectly, but for the 50% suspension a significant decrease in η_r was observed after the initial pre-shear.

As correctly pointed out,[10] migration complicates the comparison of steady shear viscosity results for noncolloidal suspensions from various researchers. Such a comparison is not the purpose of our current work, we just note that our viscosity data are somewhat higher than the results of Gadala-Maria and Acrivos,[10] which should be expected since we do not wait for the system to reach the migratory equilibrium.

Figure 8 exhibits shear-thinning behavior, most notably at the highest volume fraction. The shear thinning is also present in equilibrium curves of Gadala-Maria and Acrivos.[10] The flow curves were measured subsequently for increasing and decreasing stresses and the minimal amount of hysteresis was insufficient to relate the shear-thinning effect to shear-induced particle migration.

Recently, Zarraga *et al.*[21] have presented steady shear viscosity data from parallel plate rheometry and reported the same phenomenon. As they suggest, the explanation probably lies in the underlying suspension microstructure, but it is unclear what happens exactly. As far as we could examine, our PMMA particles can be considered as hard spheres without additional interparticle interactions. Refractive index matching eliminates van der Waals interactions even at the lowest shear rates and the large amount of salt screens off electrostatic repulsions—if present at all. Brownian motion, finally, is also extremely small for our 90 μm particles and

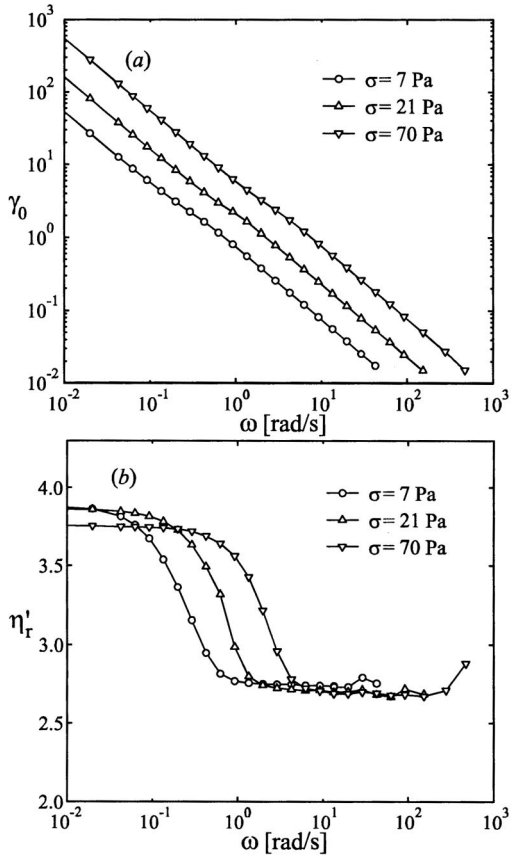

FIG. 9. Results of constant stress frequency sweeps for a 30% suspension; (a) the amplitude of the strain response, γ_0, vs angular frequency ω and (b) η_r' vs ω for varying stress values: (○) 7 Pa, (△) 21 Pa, and (▽) 70 Pa.

cannot be held responsible for the shear-thinning behavior.

The steady shear experiments were followed by dynamic measurements. Because of the controlled stress nature of the Haake RS150 rheometer, the stress amplitude of the oscillations (σ) was kept constant, while the angular frequency (ω) was varied from 0.0094 to 628 rad s^{-1} (0.0015–100 Hz). Because of constant σ, the amplitude γ_0 of the strain response varied with ω. For a sample with frequency independent rheological properties (e.g., Newtonian fluid) the relation would simply have been $\gamma_0 \sim \sigma/\omega$.

Figure 9 shows the result of frequency sweeps for different values of σ and $\phi = 0.30$. In the left graph, the strain amplitude of the response signal γ_0 is plotted versus ω. As expected, γ_0 decreases strongly with ω and for each specific value of ω the strain amplitude increases with σ. The corresponding data for the relative dynamic viscosity η_r' data are presented in the right graph and show very peculiar behavior. At low frequencies η_r' has a well-defined plateau value. Another—considerably lower—plateau is observed at high frequencies. In the intermediate regime, there is a sharp transition, which shifts with variations in the stress amplitude σ.

The two graphs of Fig. 9 suggest that the η_r' transition is determined by strain amplitude rather than by frequency. To check this hypothesis, we have plotted η_r' against γ_0 in Fig. 10 for $\phi = 0.30$ and 0.50 (note the logarithmic scale). The transitions in the dynamic viscosity curves nicely collapse for both volume fractions. A sudden change in the viscoelastic response of the suspension occurs at strain amplitudes around $\gamma_0 \sim O(1)$.

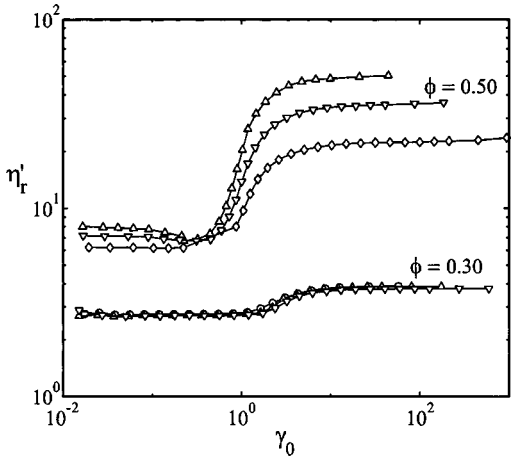

FIG. 10. Relative dynamic viscosity η_r' vs amplitude of the strain response, γ_0, measured for $\phi = 0.30$ and 0.50 in frequency sweeps at various stress levels: (○) 7 Pa, (△) 21 Pa, (▽) 70 Pa, and (◇) 210 Pa.

Figure 10 clearly shows that for our noncolloidal suspensions the dynamic viscosity η_r' strongly depends on strain amplitude γ_0. Within rheological nomenclature it would thus be more appropriate to name the quantity ''*apparent* dynamic viscosity,'' since the use of η' is generally restricted to the linear low strain regime. However, to avoid extended formulations we simply refer to η' as ''dynamic viscosity'' over the entire measurement range, referring to the out-of-phase component of the strain response signal as produced by the rheometer.

Graphs similar to Fig. 10 were obtained before,[11] but in these experiments the transitions were more gradual, most probably due to the wide range of shear rates in the parallel plate configuration which smooths out strain-dependent transitions.

A close look at the raw oscillatory signals provides more insight into the observed effects, as can be seen in Fig. 11. The graph denotes the strain response functions for a 50% suspension at various frequencies (and thus various strain

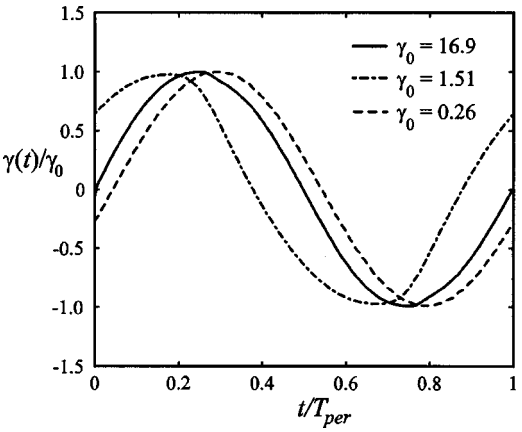

FIG. 11. Strain response signals $\gamma(t)$ for sinusoidal stress input signal (amplitude 70 Pa) at three different values of ω—and therewith γ_0—; $\phi = 0.50$ and the curves are scaled by the oscillation period T_{per} and amplitude γ_0.

amplitudes). Note that for clarity the strain signals $\gamma(t)$ have been scaled by the oscillation period T_{per} and amplitude γ_0. Unfortunately, our rheometer was unable to start its measurements at a reproducible point of the stress input signal, so that no conclusions are to be drawn from the apparent phase differences in Fig. 11.

Below the transition ($\gamma_0=0.26$ in Fig. 11) the strain response is sinusoidal and linear, so that η' is independent of γ_0 and a plateau is found. In the transitional regime the response is strongly nonharmonic: The strain response for $\gamma_0=1.51$ resembles a saw-tooth rather than a sinus. Note that the signal is asymmetrical on reversal of flow direction at the maxima of the oscillation. At very large strain values ($\gamma_0=16.9$) the material response is nearly harmonic again, at a considerably higher value of η'. Traces of nonlinear response can still be observed at the turning points where the flow direction changes, but at large amplitudes the response is dominated by a sinusoidal contribution that is responsible for the determination of η_r'. Figure 11 shows that the rheometer output for η_r' in the transitional regime has no clear physical meaning: η' is only a well-defined quantity for sinusoidal input and output. Similar nonharmonic responses were reported by Gadala-Maria and Acrivos,[10] who analyzed the raw signals of their controlled strain rheometer for $\gamma_0 \leqslant 1.05$. The authors were able to directly relate the shape of the nonlinear stress response to the buildup of shear-induced microstructure, which they also found in elegant steady shear flow reversal experiments.

The discrepancy between the two plateaus in Fig. 10 strongly increases with volume fraction, ranging from a factor 1.3 for $\phi=0.30$ up to a factor 5 for $\phi=0.50$. The location of the transition ($\gamma_{0,\mathrm{tr}}$) also varies with volume fraction, defining $\gamma_{0,\mathrm{tr}}$ as the strain amplitude at the point where η_r' is halfway between the plateau values on the log–log scale. The transition point shifts from $\gamma_{0,\mathrm{tr}}=3.0\pm0.4$ for $\phi=0.30$ to $\gamma_{0,\mathrm{tr}}=1.0\pm0.2$ for $\phi=0.50$, the errors being largely due to the variations in plateau values with stress.

VI. DISCUSSION

The results of the various experimental techniques described in the previous sections provide inspiration for consideration on their physical background. In this section we will first discuss the results of diffusion and rheology separately and then draw the parallels and provide a framework for physical interpretation.

A. Self-diffusion

The self-diffusion data under steady shear are described extremely well by an empirical fit function [Eq. (1)]. The measurements show how the average particle motion develops when monitored from a certain arbitrary starting point in time ($\dot\gamma\Delta t=0$). For very small deformations $\dot\gamma\Delta t$ the surroundings of a particle are hardly changed and particles are observed to move diffusively, characterized by a diffusion coefficient $\hat D_0$. In the particle trajectories this effect can be noticed for $\phi=0.50$ in the shape of rapid fluctuations of small amplitude. For larger deformations, $\dot\gamma\Delta t\approx1$, the initial particle configuration is distorted significantly and the average particle motion is affected accordingly. In this regime, particles are forced by the shear flow to pass their neighbors. The trajectories clearly display the associated steps of size $O(a)$. After even longer times $\dot\gamma\Delta t>1$, the correlation of the particle motion with the initial state is lost and a diffusive mode is reached, with diffusivity $\hat D_\infty$. Although the flow is in steady state macroscopically at every moment, the particle motion measured from an arbitrary starting point $\dot\gamma\Delta t=0$ reaches a ''steady'' diffusive state only after deformation $\dot\gamma\Delta t>1$.

The characteristic times that can be associated with the transition, $\hat\tau_0$, marking the end of the short-time diffusion and $\hat\tau_\infty$, marking the onset of long-time diffusion, show a different scaling with concentration, $\hat\tau_\infty\sim1$ being constant and $\hat\tau_0$ decreasing with increasing ϕ. The associated diffusion coefficients $\hat D_0$ and $\hat D_\infty$ also exhibit different dependencies on ϕ: While $\hat D_\infty$ grows strongly with ϕ at intermediate concentrations ($\phi<0.35$) and reaches a plateau value for higher volume fractions, $\hat D_0$ grows monotonically as a function of ϕ.

The ϕ dependence of the long-time self-diffusion coefficient is remarkable. As discussed in more detail in another paper,[8] this particular behavior has so far only been found experimentally. Numerical Stokesian dynamics calculations have not yet resulted in a clear numerical picture: Shear-induced diffusion data seem to depend on system size and numerical algorithm. The only theoretical attempt by Brady and Morris[14] predicts $\hat D_\infty$ to grow with ϕ up to volume fractions where flow becomes impossible. Their prediction, which is in fact an extrapolation of scaling relations in the dilute regime rather than a first principles theory, is based on the idea that diffusion should scale with the product of frequency and size of the particle displacements due to interactions. Using the contact value of the pair-distribution function $g(\mathbf{r})$, they argue that the interaction frequency should increase with volume fraction, while the step size remains more or less constant $O(a)$, thus giving rise to an increasing diffusivity.

There is recent evidence, however,[22] that in numerical Stokesian dynamics calculations at high concentrations (roughly above 30%) particle pairs tend to align in the flow direction. This effect is deduced from the appearance of peaks in the particle pair-distribution function $g(\mathbf{r})$ along the direction of flow. At high Péclet numbers the concentration of particle pairs is usually enlarged along the compressive axes of the shear flow, but recent calculations revealed the existence of additional peaks along the streamlines. The effect was not found to cause long-range order in the system (formation of particle strings), but the change in the local particle structure could very well be responsible for a decrease in the interaction frequency, since the increased number of particle pairs aligned along the streamlines effectively screens interactions with other particles on neighboring streamlines. Thus the number of interactions would be reduced with increasing volume fraction, providing an explanation for the experimentally observed plateau in $\hat D_\infty$.

To our knowledge the experimental observations of a short-time shear-induced self-diffusion are unique. Its exis-

tence is concluded from the quality of an empirical model fit to all available data. Although clear experimental evidence exists it is not straightforward to interpret the observations. The existence of an additional short-time diffusive process in itself is not strange. In Brownian suspensions a similar distinction between long- and short-time diffusion can be found: at short times the particles are rattling within the cage formed by their neighbors, the short-time self-diffusion, and only when the cage has been deformed sufficiently are particles able to undergo large displacements, characterized by a long-time self-diffusion coefficient.

Following the analogy with colloidal systems, apparently also noncolloidal systems exhibit small displacements within a ''cage'' on time scales which are so short that the configuration of particles remains unchanged ($\dot{\gamma}\Delta t \ll 1$). Two possible mechanisms have come to our mind to explain these fluctuations in the absence of Brownian motion. The first possibility is an interparticle force with a short but finite range (e.g., as a result of inevitable particle roughness in experimental systems) which at short times is able to relax the flow-induced contacts between noncolloidal particles by pushing them apart, thus giving rise to minute displacements. An alternative explanation could be found in the long-range character of the hydrodynamic forces in a sheared suspension. Each particle will not only feel the interaction with its immediate neighbors, but always experience fluctuations due to particle motion at larger distances. Fluctuations of this kind could cause diffusive displacements and would most likely be of a higher frequency than the interactions with direct neighbors, which give rise to long-time diffusion.

The ''cage'' concept is in agreement with the observed behavior of the transition time $\hat{\tau}_0$. As shown in Fig. 7 a simple calculation of the size of the cage [Eq. (4)] provides a good estimate for the upper limit of the deformation where short-time diffusion should be dominated by the large displacements of long-time self-diffusion.

The experimental observation that $\hat{D}_0$ grows with ϕ (Fig. 5) at first sight seems compatible with both mechanisms: at larger volume fractions stronger hydrodynamic fluctuations could be expected and also particles would be pushed harder toward each, which could lead to larger relaxation steps. Conclusive evidence on this topic could not be extracted from either of our experiments, but the persistent observation of $\hat{D}_0$ is quite intriguing.

B. Rheology

Steady shear and oscillatory measurements have shown that the two important parameters to characterize the results are stress and strain. The flow curves show that for increasing stress, shear-thinning occurs (Fig. 8). This effect is most probably the result of changes in microstructure. All other possible explanations seem to fail: Brownian motion is absent and the presence of interparticle forces is unlikely.

In oscillatory experiments two strain regimes can be identified in the dynamic viscosity η_r'. At small amplitudes ($\gamma_0 \ll 1$) the stress and strain signals are harmonic and a well-defined plateau exists. The particle positions remain virtually unchanged during these measurements and the microstructure at rest is probed.

For larger amplitudes [$\gamma_0 \sim O(1)$] the strain signal becomes nonharmonic (Fig. 11). The shape of this nonlinear stress response is related to the buildup of shear-induced microstructure as explained by Gadala-Maria and Acrivos.[10] They found that the typical deformation required to complete structure formation in the flow reversal measurements was $\gamma \sim 2$ and the value decreased with increasing volume fraction (see their Fig. 7). Oscillatory measurements on our suspensions corroborate their results. The characteristic strain value $\gamma_{0,\mathrm{tr}}$, which we used to define the location of the transition between the η_r' plateaus, is in quantitative agreement with the typical time scale for flow-induced structure formation as measured by Gadala-Maria and Acrivos.

At very large strain amplitudes ($\gamma_0 \gg 1$) the particles are forced into a microstructure which resembles the situation under steady shear. After reversal of the flow direction only a small fraction of the oscillation period is needed to break down and rebuild the microstructure. During the remaining part of the oscillation, the microstructure has reached a steady state and the response is ''apparently'' linear with a dynamic viscosity η_r'. This is nicely illustrated by Fig. 11, where the strain response is strongly nonlinear for intermediate strain amplitude $\gamma_0 = 1.51$ after flow reversal, while only a relatively small dimple can be observed for the large amplitude experiment $\gamma_0 = 16.9$. In absolute strain units, the region of microstructural rearrangements are of the same magnitude for both signals: $\Delta\gamma \sim 3$.

The plateau values of η_r' at high strain oscillations exhibit shear-thinning behavior that is similar to the steady shear flow curves. In particular for $\phi = 0.50$ the high strain plateau values do not overlap completely. The variations in plateau value cannot be attributed to migration: In our experiments we have repeated the full sequence of three frequency sweeps for several times overnight and the overlap between the first and last sequence at each specific stress value was excellent, the overnight variations in η_r' at a specific stress value being much smaller than variations between different stress curves.

Quantitative analysis of the low strain (high frequency) plateau, where shear-induced microstructure is absent reveals an interesting observation. In Fig. 12 we have plotted the plateau values for our noncolloidal suspensions together with literature data on colloidal suspensions.[23,24] For colloidal hard-sphere suspensions the high frequency limit of the dynamic viscosity, $\eta_{r,\infty}'$, is a well-defined quantity representing the hydrodynamic viscosity contribution at time scales where the Brownian motion is negligible, so that the equilibrium particle distribution is probed. The agreement is excellent, suggesting that the high frequency viscosity of hard sphere suspensions is independent of Péclet number.

At first glance the agreement is remarkable. For colloidal particles the Brownian motion rapidly relaxes shear-induced structure after cessation of flow, but for noncolloidal particles this force is extremely weak so that the associated relaxation processes become very slow and the particle distribution is not in thermodynamic equilibrium during the dynamic measurements. Nevertheless, within experimental

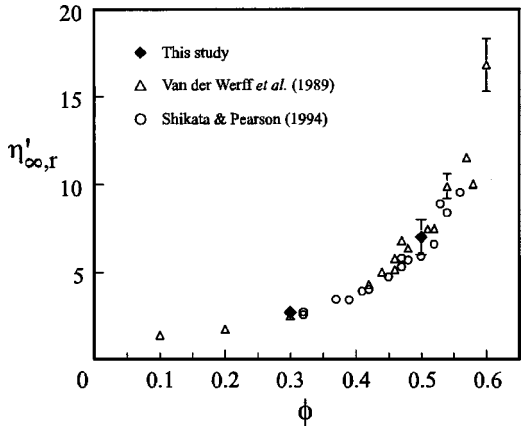

FIG. 12. Relative dynamic viscosity η_r' as a function of particle volume fraction; low strain plateau values from this study (◆) are compared to the high frequency limit as determined by Van der Werff *et al.*—Ref. 23 (○) and Shikata and Pearson—Ref. 24 (△) for colloidal hard-sphere suspensions.

errors the high frequency measurements yield the same relative dynamic viscosity for both colloidal and noncolloidal systems.

This observation can be interpreted within the theoretical framework developed by Brady and co-workers.[14] Their approach is based on analyzing the particle pair distribution function $g(\mathbf{r})$. Without going into the details, a relevant result of the analysis is the existence of a thin lubrication boundary layer around a particle of thickness $O(a\,\mathrm{Pe}^{-1})$, where Pe is the Péclet number and a the particle radius. At high concentrations the fraction of particle pairs residing within this boundary layer—described by the pair-distribution function at contact, $g(2,\theta)$—is argued to dominate the suspension stress. As a result, relaxation of this extremely thin boundary layer would be sufficient to remove the shear-induced viscosity contribution. Since the Péclet number in our noncolloidal system is very high $[O(10^{10})]$, the boundary layer is so thin that even the extremely weak residual Brownian motion or the slightest particle roughness will be strong enough to rapidly destroy the boundary layer after cessation of flow. The high-frequency viscosity is then determined by the fraction of particles that remains within the boundary layer after relaxation, which is probed in oscillatory flow. Outside the equilibrium boundary layer our noncolloidal system has not reached thermodynamical equilibrium and the distribution is nonhomogeneous. Nevertheless, the same $\eta'_{\infty,r}$ values are found for colloidal and noncolloidal systems, in accordance with the idea that the boundary layer dominates viscosity.

C. Relation between self-diffusion and rheology

In this section we compare the different observations and try to embed the results in a coherent physical interpretation. Our main aim is to provide a sound experimental basis for discussions about the microscopic processes in sheared suspensions and not to give a detailed quantitative theoretical interpretation. We want to make use of the acquired expertise by pointing out striking correspondences within our set of experiments.

At first glance the combination of studying self-diffusion and rheology might raise questions. However, both physical quantities have the same origin: the spatial distribution of particles. This can easily be shown within the formalism used by Brady and Bossis:[9]

$$\begin{bmatrix} F^H \\ S \end{bmatrix} = \begin{bmatrix} R^{Fv} & R^{FE} \\ R^{Sv} & R^{SE} \end{bmatrix} \begin{bmatrix} v^\infty - v \\ E^\infty \end{bmatrix}, \tag{5}$$

where $F^H \equiv (\mathbf{F}_1^H, \mathbf{F}_2^H, \ldots, \mathbf{F}_N^H)^\mathbf{T}$ is a vector of the hydrodynamic forces on the N particles in the system. Similar definitions apply to the stresslet vector S and the particle velocities relative to the ambient flow $v^\infty - v$. E^∞ represents the external rate of strain. The resistance matrices $R_{\alpha,\beta}$ depend on the positions of all particles in the suspension.

By partial inversion Eq. (5) can be rewritten in a more suitable form:[25]

$$\begin{bmatrix} v^\infty - v \\ S^\infty \end{bmatrix} = \begin{bmatrix} A^{vF} & A^{vE} \\ A^{SF} & A^{SE} \end{bmatrix} \begin{bmatrix} F^H \\ E^\infty \end{bmatrix}, \tag{6}$$

where the matrix elements $A_{\alpha,\beta}$ are directly related to the resistance matrices $R_{\alpha,\beta}$ and thus also depend on particle configuration only. For our noncolloidal suspension in Stokes flow and in absence of interparticle forces, the hydrodynamic force $\mathbf{F}_i^H = \mathbf{0}$ on every particle. Thus the relative velocity and stresslet are functions of the external rate of strain and the particle configuration only. Self-diffusion is directly related to the autocorrelation of $\mathbf{v}^\infty - \mathbf{v}_i$, averaged over all particles. The macroscopic viscosity can be calculated through the integral of the particle stresslet $\mathbf{S}_i$ weighted with the particle distribution function. Thus both self-diffusion and viscosity directly depend on the spatial distribution of particles.

Because of the joint background, a comparison between the experimental results is meaningful. The onset of the long-time self-diffusion regime in particle motion can be associated with the occurrence of nonlinearity in the strain response signal during dynamic viscosity measurements. Both indicate the typical strain at which excluded volume effects of neighboring particles become of importance. Indeed, there is qualitative agreement in the sense that both transitions take place for strain values of $O(1)$ and that the transition shifts to lower values for increasing volume fraction ϕ. Quantitative agreement is difficult to verify, since the definition of the transition locations is somewhat subjective.

The diffusion coefficient $\hat{D}_\infty$ and plateau in η_r' for large strain amplitudes show the effect of multiple excluded volume effects in the large deformation limit, where the initial configuration has been lost. The volume fraction dependency of these quantities shows a notable correlation: at high volume fractions the long-time diffusion levels off, while the large amplitude dynamic viscosity increases strongly. Apparently, it becomes more difficult for particles to move and deformation requires larger stresses.

In the limit of small deformation the particle configuration is hardly changed. Both $\hat{D}_0$ and $\eta'_{r,\infty}$ reflect the suspension properties under these conditions and following the correlation for diffusion and viscosity at large deformations, they should be linked. The existence of a short-time diffu-

sion requires a driving force of unknown origin; two possible explanations were provided in Sec. VI A. From oscillatory measurements we have discovered that the small amplitude viscosity $\eta'_{r,\infty}$ of colloidal suspensions is the same as the high frequency limit for noncolloidal suspensions. These results, although not yet completely understood, set the stage for further discussion on the microstructure of concentrated suspensions.

VII. CONCLUSIONS

We have experimentally studied concentrated noncolloidal suspensions under shear by employing three different techniques: particle tracking to determine the trajectories of individual particles, ensemble averaged displacements statistics, and rheometry. The techniques probe the suspension on three different levels: the microscopic particle position, the ensemble level of average motion, and the macroscopic level of mechanical properties. The combination of measurements has enabled us to find a number of intriguing results which altogether provide a coherent qualitative physical picture of the microscopic structure in sheared suspensions.

Particle tracking revealed that for medium concentrated suspensions (30%) the particle trajectories are very smooth with distinct displacements due to interactions with neighboring particles on the characteristic time scale of the shear flow [$\dot{\gamma}\Delta t \sim O(1)$]. The size of the displacements in both the vorticity and velocity direction was $O(a)$, which is in agreement with shear-induced diffusion experiments. The fluctuations in the velocity direction are more pronounced and this could be attributed to the coupling of diffusion in the velocity gradient direction with the convective flow.

For a highly concentrated 50% suspension the picture is similar, although the frequency and size of the displacements are slightly larger and the particles exhibit additional fluctuations of a shorter time scale superimposed on the ''slow'' fluctuations.

A more detailed analysis of previously reported shear-induced self-diffusion data[8] showed that in addition to the well-known long-time diffusivity the motion at the shortest experimentally accessible time scales ($\dot{\gamma}\Delta t < 0.10$) is also of diffusive nature. This phenomenon has not been observed before.

Our data over the entire range of time could be characterized very well by means of an empirical model. The model was chosen in such a way that a minimum of physically meaningful parameters was sufficient to describe the data, i.e., two dimensionless diffusion coefficients—$\hat{D}_0$ and $\hat{D}_\infty$—, two transition times—$\hat{\tau}_0$ and $\hat{\tau}_\infty$—, and an unimportant, but physically meaningful parameter c_4.

The long-time diffusion coefficient $\hat{D}_\infty$ exhibits a peculiar dependence on volume fraction: up to $\phi = 0.35$ it strongly increases, above this volume fraction $\hat{D}_\infty$ levels off and even has the tendency to go down at 0.50. Experimentally this behavior has been reported before with two different techniques.[6,8] However, because of contradictory numerical and theoretical results, its origin is still subject of discussion. The characteristic onset of long-time diffusion, $\hat{\tau}_\infty$ (for a definition see Fig. 7), is more or less constant within the experimental errors at a value $\tau \approx 1$—expressed in strain units—as would be expected from a phenomenon driven by particle interactions in shear flow.

The short-time diffusive process was described by the diffusion coefficient $\hat{D}_0$, which is significantly smaller than $\hat{D}_\infty$ and increases with ϕ. We have no unambiguous interpretation of this quantity, but the underlying displacements occur on a time scale on which the configuration of neighboring particles has not changed. The time scale of this diffusive process is much shorter, $\hat{\tau}_0 \ll \hat{\tau}_\infty$, and quantitatively the values of $\hat{\tau}_0$ are in agreement with the concept of ''caging'' at short times. At longer times, direct hydrodynamic interactions with neighboring particles lead to larger displacements and the long-time self-diffusion becomes dominant.

In controlled stress oscillatory experiments a strong dependence of the (apparent) relative dynamic viscosity η'_r on the strain amplitude γ_0 was noticed. At high strain values ($\gamma_0 \gg 1$) a well-defined plateau of η'_r exists and a much lower plateau was found for small amplitudes ($\gamma_0 \ll 1$). The difference between the two plateaus was attributed to shear-induced structure at high deformations, when particles are driven closely together, thus giving rise to an extra contribution to the viscosity. The structure is generally characterized by the pair-distribution function $g_2(\mathbf{r})$ in the thin boundary layer around the particle.[14] During low strain oscillations this structure related viscosity contribution disappeared, leaving a lower η'_r plateau which coincides perfectly with the high frequency (and thus low strain) limit $\eta'_{\infty,r}$ as observed in Brownian suspensions.[23,24] This correspondence suggests that even in noncolloidal suspensions the boundary layer is rapidly destroyed after cessation of flow. According to the theoretical scaling of Brady and Morris,[14] the small residual Brownian force would be sufficient to eliminate the extremely thin boundary layer structure, so that the boundary layer reaches equilibrium almost instantly. The distribution of particles outside the boundary layer is apparently less important for the high frequency limit of η'_r. In noncolloidal suspensions the particle distribution outside the boundary layer does not reach equilibrium during oscillatory measurements.

ACKNOWLEDGMENT

The work described in this paper was supported by the Foundation for Fundamental Research on Matter (FOM) in the Netherlands.

[1] A. Acrivos, J. Rheol. **39**, 813 (1995).
[2] D. Leighton and A. Acrivos, J. Fluid Mech. **177**, 109 (1987).
[3] D. Leighton and A. Acrivos, J. Fluid Mech. **181**, 415 (1987).
[4] R. Davis, J. Fluid Mech. **310**, 325 (1996).
[5] E. Eckstein, D. Bailey, and A. Shapiro, J. Fluid Mech. **79**, 191 (1977).
[6] S. Phan and D. Leighton (unpublished).
[7] V. Breedveld, D. van den Ende, A. Tripathi, and A. Acrivos, J. Fluid Mech. **375**, 297 (1998).
[8] V. Breedveld, D. van den Ende, M. Bosscher, R. J. J. Jongschaap, and J. Mellema, Phys. Rev. E **63**, 021403 (2001).
[9] J. Brady and G. Bossis, Annu. Rev. Fluid Mech. **20**, 111 (1988).
[10] F. Gadala-Maria and A. Acrivos, J. Rheol. **24**, 799 (1980).
[11] P. Gondret, L. Petit, and G. Bossis, in Proceedings of the XIIth International Conference on Rheology, edited by A. Ait-Kadi, J. Dealy, D. James,

and M. Williams, Laval University, Quebec City, Quebec, 18–23 August 1996, pp. 554–555.
[12] S. C. Jana, B. Kapoor, and A. Acrivos, J. Rheol. **39**, 1123 (1995).
[13] K. Knipmeyer and D. Pine (private communication).
[14] J. Brady and J. Morris, J. Fluid Mech. **348**, 103 (1997).
[15] F. da Cunha and E. Hinch, J. Fluid Mech. **309**, 211 (1996).
[16] Y. Wang, R. Mauri, and A. Acrivos, J. Fluid Mech. **327**, 255 (1996).
[17] R. Pesche, Ph.D. thesis, Universite de Nice-Sophia Antipolis, France, 1998.
[18] D. Foss and J. Brady, J. Fluid Mech. **401**, 243 (1999).
[19] M. Cross, J. Colloid Sci. **20**, 417 (1965).
[20] F. Gadala-Maria, Ph.D. thesis, Stanford University, 1979.
[21] I. Zarraga, D. Hill, and D. Leighton, J. Rheol. **44**, 185 (2000).
[22] B. Katyal and J. Morris, J. Chem. Phys. (submitted).
[23] J. van der Werff, C. de Kruif, C. Blom, and J. Mellema, Phys. Rev. A **39**, 795 (1989).
[24] T. Shikata and D. Pearson, J. Rheol. **38**, 601 (1994).
[25] R. Jongschaap and J. Mellema, J. Rheol. **39**, 953 (1995).